IEEE Open Journal of Antennas and Propagation

Received 28 February 2022; revised 12 April 2022; accepted 17 April 2022. Date of publication XX Month XXXX; date of current version XX Month XXXX.

Digital Object Identifier 10.1109/OAJPE.2020.2976889

An Indirect Method for an Alternate Perspective to Dispersion Diagrams of Magnetoinductive Waveguides

VIGYANSHU MISHRA, MEMBER, IEEE, AND ASIMINA KIOURTI, SENIOR MEMBER, IEEE

ElectroScience Laboratory, Department of Electrical and Computer Engineering, The Ohio State University, Columbus, OH 43212 USA

CORRESPONDING AUTHOR: Vigyanshu Mishra (e-mail: mishra.186@osu.edu).

This work was supported by the National Science Foundation under Grant 2053318.

ABSTRACT The dispersion equation of magnetoinductive waveguides (MIWs) is traditionally solved directly for the propagation constant (γ) to obtain diagrams for the attenuation (α) and phase (β) constants vs. angular frequency (ω). Here, we introduce an indirect method of solving the equation, in two steps. By doing so, additional information and insights are provided in the intermediate step, not available via the traditional direct method. The first step of the reported approach splits α into attenuation constant in the propagating passband (α') and the evanescent stopband (β''); and β into phase constant in the propagating passband (β') and the evanescent stopband (α''). The resulting four diagrams can then be suitably combined in the second step to obtain α and β diagrams that show excellent congruence with the direct method. The additional information obtained is fundamental in nature and can be utilized to aid in the understanding and design of MIWs. For instance, it can help formulate quantitative criteria to precisely segregate the propagating passband from the evanescent stopband, which further enables a theoretical bound for the propagating mode of operation. The reported indirect method is generic and can be used for any type of MIW structure and any order of coupling.

INDEX TERMS Dispersion diagrams, dispersion equation, direct method, indirect method, magnetoinductive waveguides, magnetoinductive waves, metamaterials, periodic structures.

I. INTRODUCTION

Magnetoinductive Waveguides (MIWs) have been an active subject of research since their conception in the context of metamaterials [1], [2]. MIWs are formed by periodic arrangements of electrically small resonant loops that support propagation of magnetoinductive waves (MI waves) [1], [2]. These are slow wave structures and are sometimes referred to as magnetic metamaterials [2]–[4]. MI waves are also observed in other periodic structures/metamaterials that are formed by unit elements having characteristics similar to electrically small resonant loops, such as split ring resonators [5], swiss roll structures [6], etc. These have been extensively studied and applied in imaging [7], radiofrequency identification [8], sensing [9]–[11], wireless power transfer [4], and wireless body area networks (WBANs) [12], [13].

Dispersion diagrams characterize MIWs in a fundamental way and, hence, play a crucial role in laying the foundations of their design. To obtain these dispersion diagrams, the (non-linear and complex) dispersion equation [1]–[3], [10], [14] needs to be solved. Following the traditional way, the equation is solved directly for the propagation constant (γ) as a function of angular frequency (ω) to obtain the dispersion diagram. This γ is typically complex due to loss ($= \alpha + j\beta$) and can be split into real and imaginary parts to obtain separate diagrams for both α (attenuation constant) and β (phase constant) as a function of ω. Since the solution is obtained directly in a single step, we term this method as direct method. Results obtained via this theoretical method have been shown to match with experimental results [14], confirming its accuracy. Hence, the direct method can be used as a reference to compare and validate against.

In this work, we propose an indirect method of solving the dispersion equation that provides additional information and insights, not available via the direct method [see Fig. 1]. We term the method as indirect as it requires two steps to obtain the dispersion diagram. Specifically, the first step derives the attenuation constant in the propagating passband (α'), phase constant in the propagating passband (β'), attenuation constant in the evanescent stopband (β''), and phase constant in the evanescent stopband (α''). These four components that are not available via the direct method govern different regions of the dispersion diagram, can precisely segregate the propagating passband and evanescent stopband regions of the

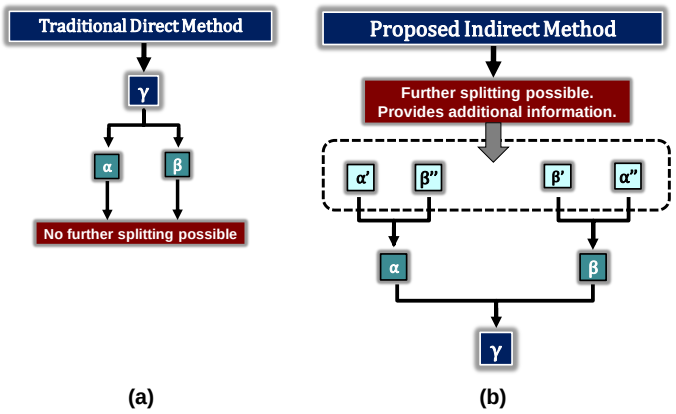

FIGURE 1. **Comparison of (a) traditional direct and (b) proposed indirect methods.**

diagram, and provide four separate diagrams for $\alpha', \beta', \alpha''$, and β'' vs. ω. They can also be recombined in the second step of the method to derive α and β that are in excellent congruence with the direct method. It is worth emphasizing that the proposed method does not only trivially separate complex γ into α and β (which is also possible via the direct method), but also, further splits α and β into their constitutive components/constants (α', α'', β', and β'') [see Fig. 1].

Apart from providing a more detailed picture that provides intuitive understanding, the reported indirect method utilizes four new obtained constants to formulate very simple quantitative criteria that precisely determine the propagating and evanescent regions, hence creating theoretical bounds for the propagating mode of operation. In short, the method provides useful new theoretical information that can complement the direct method and aid in the future development of MIW based technologies. The method is generic in nature, applies to any MIW design, and can provide solution for any order of coupling.

The rest of the paper is organized as follows. Section II provides a brief background on MIWs, the dispersion equation, and the direct method. Section III describes the proposed indirect method. Section IV discusses the MIW designs that are used to demonstrate the indirect method. Results are presented in Section V along with important discussions. Section VI concludes the work.

II. MAGNETOINDUCTIVE WAVEGUIDES (MIWS), DISPERSION EQUATION AND THE DIRECT METHOD

MIWs are formed by placing multiple conductive and electrically small resonant loops in series, with a certain gap between them, such that there exists mutual coupling to allow for propagation of MI waves. Fig. 2 shows two basic 1-D configurations: (a) planar (planes of all loops lie along the same plane, Fig. 2(a)) [2], and (b) axial (axes of loops are aligned along the same axis, Fig. 2(b)) [2]. Here, loop 1 acts as a source/transmitter whose time-varying current produces time-varying magnetic flux that gets coupled to neighboring loops and induces voltage via Faraday's law of induction. This induced voltage leads to current flow in the neighboring loops and the process continues until current is induced on

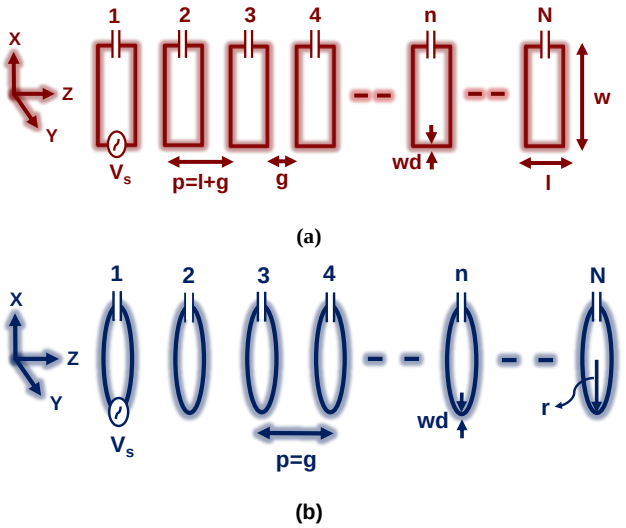

FIGURE 2. **1-D Magnetoinductive waveguide (MIW) in two different configurations, (a) planar, and (b) axial.**

the last (N^{th}) loop, thereby leading to propagating MI waves. These MI waves are characterized via the dispersion equation that is given by [2]:

$$\left(\frac{\omega_o}{\omega}\right)^2 - 1 + \frac{j}{Q} = \sum_{m=1}^{U} K_m \cosh(m\gamma p), \qquad (1)$$

where $\omega_o = 1/\sqrt{LC}$ is the resonant angular frequency of each loop (L is the self-inductance of each loop and C is the lumped capacitance added to make the loops resonant), $Q = \omega L/R$ is the quality factor of each loop (ω is the operating angular frequency and R is the resistance of each individual loop), m represents the order of coupling (e.g. $m = 1$ for coupling between loop 1 and 2, $m = 2$ for coupling between loop 1 and 3, and so on), U represents the highest order of coupling considered such that $1 \leq U \leq$N-1, $K_m = 2M_m/L$ (where M_m is the mutual inductance between two loops separated by $(m-1)$ number of loops), $\gamma = \alpha + j\beta$ is the propagation constant (where α is the attenuation constant and β is the phase constant or wavenumber), and p represents the period of the structure that is uniform across the waveguide length ($p = l + g$ for planar and $p = g$ for axial per Fig. 2).

The traditional direct method directly solves (1) for γ (or, equivalently, α and β) to obtain dispersion diagrams [1], [2], [10], [14]. We term it as direct method as it can directly provide the solution in a single step, distinguishing it from the proposed indirect method. The direct method is robust, accurate, and experimentally validated [14], hence we use it as a reference to validate the results obtained via the proposed indirect method.

III. PROPOSED INDIRECT METHOD

Contrary to the direct method, the proposed indirect method solves Eq. (1) in a two-step process. As mentioned in Section I, significance lies in the calculation of constituent components of α and β which provide additional information and perspective, not possible via the direct method. For the

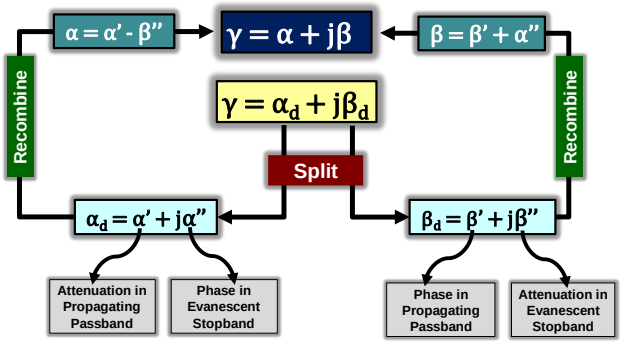

FIGURE 3. Schematic summarizing the proposed indirect method.

first/intermediate step, we solve by substituting $\gamma = \alpha_d + j\beta_d$ in (1) and expand using the standard trigonometric identity. Note that we use α_d and β_d to represent dummy variables instead of the actual α and β. This choice will become clear later. It is because of this reason that α and β are not directly obtained in the first step itself. By doing so, the m^{th} term on the right hand side of (1) yields:

$$\begin{aligned} K_m \cosh(m\alpha_d p + jm\beta_d p) \\ = K_m(\cosh(m\alpha_d p)\cos(m\beta_d p) \\ + j\sinh(m\alpha_d p)\sin(m\beta_d p)). \end{aligned} \quad (2)$$

Now, substituting (2) in (1), and equating the real and imaginary parts leads to two separate equations:

$$\left(\frac{\omega_o}{\omega}\right)^2 - 1 = \sum_{m=1}^{U} K_m \cosh(m\alpha_d p)\cos(m\beta_d p), \quad (3)$$

$$\frac{1}{Q} = \sum_{m=1}^{U} K_m \sinh(m\alpha_d p)\sin(m\beta_d p). \quad (4)$$

Both of these equations contain all three variables of interest (ω, α_d, β_d). To solve it analytically further, we introduce an approximation, $|m\alpha_d p|$ <<1, which remains valid for all required higher orders as $|\alpha_d p| \ll 1 \; \forall \; \omega/\omega_o$ for all solutions (primary and evanescent branches), and its value further reduces as m increases. Note that the approximation is valid across the frequency in both passband and stopband because $\alpha_d \neq \alpha$ as will become clear later. After incorporating the approximation, (3) and (4), respectively, reduce to:

$$\begin{aligned} \left(\frac{\omega_o}{\omega}\right)^2 - 1 = \sum_{m=1}^{U} K_m \cos(m\beta_d p) \\ = \sum_{m=1}^{U} K_m \, T_m(\cos(\beta_d p)), \end{aligned} \quad (5)$$

$$\frac{1}{Q} = \sum_{m=1}^{U} K_m m\alpha_d p \sin(m\beta_d p). \quad (6)$$

As seen, the right hand side of (5) has two equivalent forms, where $\cos(m\beta_d p)$ is a Chebyshev polynomial of first kind, $T_m(\cos\beta_d p)$, yielding a polynomial equation. As such, (5) can be used to find an explicit relation for $\beta_d p$ in terms of ω, which will be different for different values of U. The obtained expression for $\beta_d p$ can be substituted in the following equation (obtained by rearranging (6)) to get the explicit relation between $\alpha_d p$ and ω:

$$\alpha_d p = \left(Q \sum_{m=1}^{U} mK_m \sin(m\beta_d p)\right)^{-1}. \quad (7)$$

Equations (5) and (7) are generic analytical explicit expressions that can be solved for different values of ω to yield dispersion diagrams for any value of U. This will lead to U different solutions/branches with each branch taking into account the U^{th} order of coupling same as the direct method. However, α_d and β_d are not restricted to real numbers across different values of ω, and hence are more appropriately represented as:

$$\gamma = \alpha_d + j\beta_d = (\alpha' + j\alpha'') + j(\beta' + j\beta''). \quad (8)$$

This is the intermediate step that demonstrates the splitting/segregation part of the indirect method [see Fig. 3]. In the second step, we can obtain values of α and β. For this, we have to rearrange equation (8) into real and imaginary parts and recombine to get [see Fig. 3]:

$$\gamma = (\alpha' - \beta'') + j(\beta' + \alpha'') = \alpha + j\beta. \quad (9)$$

This explains our initial choice of the dummy variables α_d and β_d that is required to split α and β into further finer components ($\alpha \rightarrow \alpha', \beta''$ and $\beta \rightarrow \beta', \alpha''$). Here, (9) describes the required appropriate combination of finer components needed to yield the values of α and β. These can then always be combined to find γ ($= \alpha + j\beta$). Thus, the constants are derived in the opposite order in the direct vs. the indirect method [see Fig. 1]

As will be demonstrated in detail in Section V, the abovementioned segregation enables more in-depth and intuitive understanding of the physical phenomenon and provides additional information that is not possible with the direct method. Particularly, (i) it clearly segregates the propagating and evanescent parts in the dispersion characteristics and hence the passband and stopband, respectively, thereby providing a clear distinction between the two, (ii) α' provides information about attenuation in the propagating passband, (iii) α'' provides information about phase in the evanescent stopband, (iv) β' provides information about phase in the propagating passband, (v) β'' provides information about attenuation in the evanescent stopband [see Fig. 3], (vi) it provides an easier identification between primary and evanescent branches, and (vii) it provides an alternative way of obtaining and understanding dispersion diagrams.

IV. MIW DESIGNS FOR DEMONSTRATING THE INDIRECT METHOD

To obtain the dispersion diagrams using either the direct or indirect methods of Section III, one needs to calculate resistance (R) and inductance (L) of the loop, capacitance (C) decided by the desired resonant angular frequency ($\omega_o = (LC)^{-1/2}$), and mutual inductance (M) between two loops.

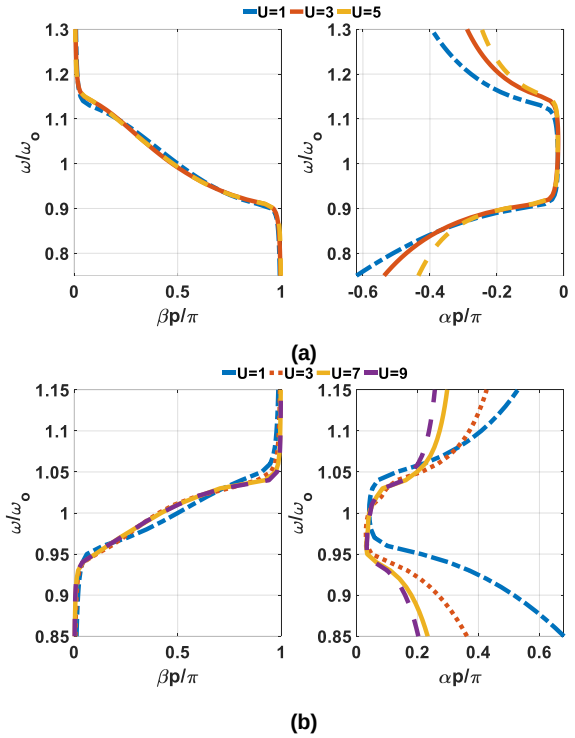

FIGURE 4. Results converge at (a) 3rd order for planar design, and (b) 7th order for axial design.

These parameters depend on the design of the MIW. Note that any MIW design can be selected to obtain these parameters as both direct and indirect methods are independent of the exact details of the design itself. Still, we select two different types of designs to cover different scenarios that can arise while obtaining dispersion diagrams (as will become more clear in Section V). Hence, without loss in generality, we consider the designs inspired from [12] for planar type and from [13] for axial type that were used to implement wireless body area networks (WBANs). The planar design includes rectangular loops made of copper with wire diameter (wd) = 0.0254 cm, length (l) = 3.5 cm, width (w) = 9.1 cm, and gap (g) = 0.25 cm [see Fig. 2(a)]. The axial design consists of resonant circular loops made of copper with wd = 0.0254 cm, radius (r) = 4 cm, and gap between the loops (g=p) = 5 cm [see Fig. 2(b)]. The planar design is implemented on a cuboidal torso, while the axial design on a cylindrical limb, with 2/3 muscle used to emulate the average human tissue properties [12], [13].

For f_o= 41.32 MHz [12], [13] we get, R=0.85 Ω, L=260.28 nH, C=57 pF, M_1=-28.36 nH, M_2=-2.21 nH, M_3=-0.69 nH M_4=-0.30 nH and M_5=-0.16 nH for planar design; and R=0.923 Ω, L=302.7 nH, C=49 pF, M_1=13.53 nH, M_2=3.34 nH, and M_3=1.21 nH, M_4= 0.55 nH, M_5= 0.30 nH, M_6= 0.18 nH, M_7= 0.11 nH, M_8= 0.079 nH, and M_9= 0.056 nH for axial design. These parameters are obtained using the CST® full-wave electromagnetic solver [15]. Dispersion diagrams obtained via the direct method for different orders of coupling (i.e. different values of U) for both planar and axial designs are shown in Fig. 4(a) and (b) respectively. Clearly, the planar design converges for 3rd order and axial design for 7th order. Hence, planar design with 3rd order (U = 3) and axial design with 7th (U = 7) order are used to demonstrate the results obtained via the indirect method in Section V. Note that the sign of α is negative for the planar design because it supports backward waves (negative group velocity) while it is positive for the axial design as it supports forward waves (positive group velocity). Conventionally, the absolute value of α is plotted to represent loss in case of planar design in literature [16]. However, here results are considered with sign to validate and demonstrate the correctness of indirect method even on this aspect.

V. RESULTS AND DISCUSSIONS

A. SEGREGATED COMPONENTS AND DISPERSION DIAGRAMS

Here, we present the diagrams of α, β and their segregated components as obtained via the two-step process of the indirect method. As established in Section IV, 3rd order (U = 3) for planar and 7th order (U = 7) for axial solutions are considered to obtain the dispersion characteristics. Following the discussion in Section III, planar design will have 3, while axial will have 7 branches. For both designs, only one of these is the primary branch that supports both propagating and evanescent waves, while the remaining solutions are completely evanescent in nature. This primary branch is usually of prime importance and is used for the demonstration of the method. Additionally, the direct method is used as a reference to validate the diagrams obtained via the indirect method. Results of the indirect method are presented in the order they are obtained in the two-step process.

The first step (or intermediate step) of the indirect method involves solving (5) and (7) to obtain (8) which provides α', α'', β', and β'' [see Section III and Fig. 3]. Referring to (9), it is clear that while β' and α'' are components of β, α' and β'' are components of α. These split components can be recombined in the second step, according to (9), to obtain the complete dispersion diagram. Fig. 5 plots results for both planar (Fig. 5(a) and (b)) and axial (Fig. 5(c) and (d)) designs. Each of these consist of the split components, their recombination according to (9) to obtain the complete diagrams of α or β, and validation against the direct method. Results clearly demonstrate the ability of the indirect method to segregate each plot into propagating and evanescent plots which can be combined according to (9) to obtain the complete α and β diagrams.

Note that, irrespective of different signs of α for planar and axial designs, the method is robust and produces correct results using the same procedure. Also, it can provide solution for any order (3rd for planar and 7th for axial here), and is applicable to any type of MIW design. In short, the method is generic, similar to the direct method, while also providing additional information that is not available by the direct method.

Referring to Fig. 5(a) and (c), β' and α'' govern propagation and evanescent characteristics, respectively, within the dispersion diagram. The value of β' directly contributes to β in the propagating passband region and is fixed at 0 or 1 in the evanescent stopband region. On the

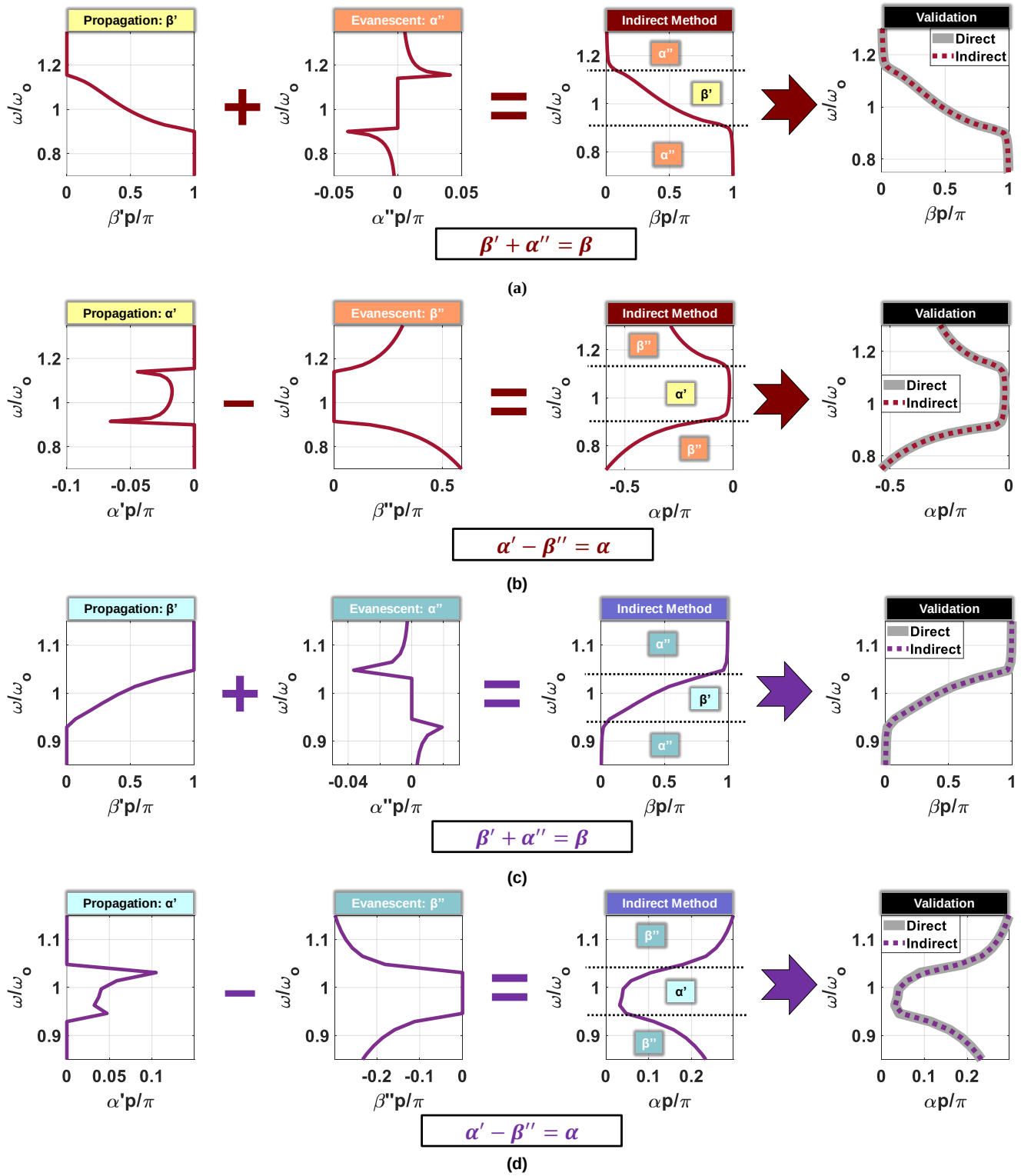

FIGURE 5. **Results depicting diagrams for segregated components of α and β, i.e. $\alpha', \alpha'', \beta'$, and β'' which govern different regions of dispersion diagram; their appropriate recombination (along with governing equations) to yield complete diagrams of α and β via indirect method; and excellent congruence with complete diagrams obtained via traditional direct method. Specifically, (a) plot of β', α'', and their recombination to yield β along with validation against direct method for 3rd order planar design, (b) plot of α', β'', and their recombination to yield α along with validation against direct method for 3rd order planar design, (c) plot of β', α'', and their recombination to yield β along with validation against direct method for 7th order axial design, and (d) plot of α', β'', and their recombination to yield α along with validation against direct method for 7th order axial design. Method is generic and applicable to any order of coupling and any type of MIW design.**

contrary, α'' directly contributes to β in the evanescent stopband and is fixed at 0 value in the propagating passband. Similarly, referring to Fig. 5(b) and (d), α' and β'' govern propagation and evanescent characteristics, respectively,

within the attenuation (α) plot. The value of α' directly contributes to α in the propagating passband and is fixed at 0 in the evanescent stopband. On the flip side, β'' directly contributes to α in the evanescent stopband and is fixed at 0 in the propagating passband. This provides a clear and precise theoretical demarcation of propagating and evanescent regions within a dispersion diagram. This information can be used for multiple purposes. For example, it can enable formulation of quantitative theoretical criteria to precisely distinguish the propagating and evanescent parts in the dispersion diagram (more details in Section V.B). Due to the above characteristics, one can also precisely distinguish the propagation part from the evanescent part merely by looking at the four new diagrams (see Fig. 5). This was not possible via the direct method.

We emphasize that the major significance of the indirect method does not lie in obtaining the dispersion diagram which can also be done by the traditional direct method. Rather, significance lies in the additional information, new insights and perspective to the dispersion diagrams. The aim of validating the complete α and β diagrams obtained via the indirect method vs. the direct method is to show that the segregated components obtained are indeed correct as their recombination produces the right α and β diagrams.

B. THEORETICAL CRITERIA AND BOUNDS: PROPAGATING AND EVANESCENT REGIONS AND BANDWIDTH EVALUATION

Utilizing the information in Section V.A, a simple theoretical criterion can be formulated for distinguishing propagation and evanescent regions quantitatively. For the propagating passband:

$$\alpha'' = \beta'' = 0, \tag{10}$$

i.e., α_d and β_d are purely real. And, for the evanescent stopband:

$$\alpha' = 0, and\ \beta' = 0\ or\ 1, \tag{11}$$

i.e., α_d and β_d are either purely imaginary or β_d is complex with real part fixed at 1.

Both (10) and (11), and the reason why each component governs particular part can be understood intuitively by observing (8). When we are in the propagating passband region, α_d and β_d are purely real and these provide us with the required solutions directly for the attenuation and phase constant, respectively. However, as we enter the evanescent stopband region, α_d and β_d are either purely imaginary or β_d is complex with real part fixed at 1. Now, in any wave propagation mechanism, if the phase constant becomes imaginary, it represents loss and also indicates that the wave has switched from propagation to evanescent mode. Similarly, if the attenuation constant becomes imaginary, it would represent the phase constant of that corresponding evanescent mode. Thus, the reason why different components govern different regions of the diagram is not random.

One immediate utility of the abovementioned criterion is in evaluating a theoretical bound on the bandwidth of propagation. The range of ω/ω_o values for which (10) is satisfied provides this bound. This can be easily obtained from any one of the four segregated component plots where (10) is satisfied. For instance, for the planar design, the bound is $0.91 \leq \omega/\omega_o \leq 1.147$, which provides fractional bandwidth of 23.7%. Similarly, for the axial design, the bound is $0.94 \leq \omega/\omega_o \leq 1.038$ which provides fractional bandwidth of 9.8%. This determines a strict theoretical bound on the propagating bandwidth, meaning any bandwidth considered outside this, will not be governed strictly by the propagating mode of operation. Note that these criteria and bounds are equally applicable on all other parameters that can be obtained for MIWs, such as group velocity.

C. DISCUSSIONS

Although results for the primary branch are demonstrated, the indirect method also produces evanescent branches similar to the direct method. In fact, it is relatively easier to identify evanescent branches using the indirect method. For all the evanescent solutions, the values of α_d and β_d are complex for all ω. This is not the case for the primary branch, thereby creating a clear distinction. In contrast, for the direct method, γ is always complex for both primary and evanescent branches and only a close observation at the exact values helps distinguish the primary branch from evanescent branches.

In general, the additional information brought forward by the indirect method provides useful insights. This information is theoretical in nature and hence can find utility in enabling better understanding and for any application of MIWs. Although results are demonstrated for 1-D waveguides, they can be extended to higher dimensions as well. It is worth noting, however, that the indirect method does have a fundamental limitation. Due to the inherent nature of recombining the constituent parts of α and β, there exists a discontinuity at the junction where α' and β'' are recombined for the α plot, and where β' and α'' are recombined for the β plot. Hence, the curves obtained are not as smooth and continuous as those obtained via the direct method at these junctions. Hence, it is important to note that the indirect method is not proposed as a replacement to the direct method for obtaining dispersion diagrams, but rather to provide a complementary way to gather more information, insights, intuitive deductions, and understanding from the dispersion diagram, in addition to obtaining the dispersion diagram itself.

In practical applications of MIWs, finite length of the waveguide and fixed impedance terminations can lead to reflections and standing waves. These will have to be further incorporated in the solution to obtain a more accurate practical solution of the problem irrespective of the method (direct or indirect) employed.

VI. CONCLUSION

In this work, we introduced a new indirect method that provides an alternate perspective on the dispersion diagrams of MIWs. Novelty of the method lies in a two-step process that provides additional useful information that is not possible by the single-step traditional direct method. The demonstration and validation of the method was performed

using two types of MIW designs, viz. planar and axial implemented for WBANs. The traditional direct method was used as a reference for validation purposes. The first step of the indirect method was shown to be capable of splitting the attenuation constant (α) and phase constant (β) into their constituent components (α', β'') and (β', α''), respectively. These components were shown to govern different regions of the dispersion diagram and, consequently, segregate the propagating passband and evanescent stopbands precisely. This helps to view the propagation and evanescent characteristics within the same diagram separately. In the second step, these components were shown to be appropriately combined to yield complete diagrams of α and β which demonstrated excellent agreement with those obtained via the direct method.

The additional information obtained by the constituent components was shown to provide useful insights and quantitative criteria for accurately distinguishing different regions in the diagram. This helps establish accurate theoretical bounds within which propagation happens. The additional theoretical information provided by the indirect method can be further utilized in various other ways to complement the direct method and aid in enhancing the understanding and design of MIWs in the future.

ACKNOWLEDGEMENT

Authors would like to thank Mr. Julio Nicolini and Mr. Daniel Ospina Acero for the fruitful discussions. This work was supported by the National Science Foundation under award number 2053318.

REFERENCES

[1] E. Shamonina, V. A. Kalinin, K. H. Ringhofer, and L. Solymar, "Magneto-inductive waveguide," *Electron. Lett.*, vol. 38, no. 8, pp. 371–373, Apr. 2002.

[2] E. Shamonina, V. A. Kalinin, K. H. Ringhofer, and L. Solymar, "Magnetoinductive waves in one, two, and three dimensions," *J. Appl. Phys.*, vol. 92, no. 10, pp. 6252–6261, Oct. 2002.

[3] C. J. Stevens, C. W. T. Chan, K. Stamatis, and D. J. Edwards, "Magnetic Metamaterials as 1-D Data Transfer Channels: An Application for Magneto-Inductive Waves," *IEEE Trans. Microw. Theory Tech.*, vol. 58, no. 5, pp. 1248–1256, May 2010.

[4] C. J. Stevens, "Magnetoinductive Waves and Wireless Power Transfer," *IEEE Trans. Power Electron.*, vol. 30, no. 11, pp. 6182–6190, Nov. 2015.

[5] I. V. Shadrivov, A. N. Reznik, and Y. S. Kivshar, "Magnetoinductive waves in arrays of split-ring resonators," *Phys. B Condens. Matter*, vol. 394, no. 2, pp. 180–183, May 2007.

[6] M. C. K. Wiltshire, E. Shamonina, I. R. Young, and L. Solymar, "Experimental and theoretical study of magneto-inductive waves supported by one-dimensional arrays of 'swiss rolls,'" *J. Appl. Phys.*, vol. 95, no. 8, pp. 4488–4493, Mar. 2004.

[7] O. Sydoruk *et al.*, "Mechanism of subwavelength imaging with bilayered magnetic metamaterials: Theory and experiment," *J. Appl. Phys.*, vol. 101, no. 7, p. 073903, Apr. 2007.

[8] F. J. Herraiz-Martinez, F. Paredes, G. Zamora Gonzalez, F. Martin, and J. Bonache, "Printed Magnetoinductive-Wave (MIW) Delay Lines for Chipless RFID Applications," *IEEE Trans. Antennas Propag.*, vol. 60, no. 11, pp. 5075–5082, Nov. 2012.

[9] J. Yan, C. J. Stevens, and E. Shamonina, "A Metamaterial Position Sensor Based on Magnetoinductive Waves," *IEEE Open J. Antennas Propag.*, vol. 2, pp. 259–268, 2021.

[10] Y. Chen, "Design of magneto-inductive waveguide for sensing applications," Ph. D. dissertation, Dept. Elec. Eng., Univ. of Texas, Austin, TX, USA, 2014.

[11] T. Trivedi, Y. Chen, I. A. D. Williamson, P. Pasupathy, and D. P. Neikirk, "Group Velocity Estimation and Defect Localization in Magneto-Inductive Waveguides," *IEEE Trans. Microw. Theory Tech.*, vol. 69, no. 4, pp. 2072–2077, Apr. 2021.

[12] V. Mishra and A. Kiourti, "Wearable Planar Magnetoinductive Waveguide: A Low-Loss Approach to WBANs," *IEEE Trans. Antennas Propag.*, vol. 69, no. 11, pp. 7278–7289, Nov. 2021.

[13] V. Mishra and A. Kiourti, "Wearable Magnetoinductive Waveguide for Low-Loss Wireless Body Area Networks," *IEEE Trans. Antennas Propag.*, vol. 69, no. 5, pp. 2864–2876, May 2021.

[14] R. R. A. Syms, O. Sydoruk, E. Shamonina, and L. Solymar, "Higher order interactions in magneto-inductive waveguides," *Metamaterials*, vol. 1, no. 1, pp. 44–51, Mar. 2007.

[15] "Electromagnetic Simulation Solvers | CST Studio Suite." Accessed: Feb. 28, 2022. [Online]. Available: https://www.3ds.com/products-services/simulia/products/cst-studio-suite/solvers/

[16] R. R. A. Syms, T. Floume, I. R. Young, L. Solymar, and M. Rea, "Flexible magnetoinductive ring MRI detector: Design for invariant nearest-neighbour coupling," *Metamaterials*, vol. 4, no. 1, pp. 1–14, May 2010.